Surface Reaction Simulations for Battery Materials through Sample-Based Quantum Diagonalization and Local Embedding

Marco Antonio Barroca^{1,6}, Tanvi Gujarati², Vidushi Sharma³, Rodrigo Neumann Barros Ferreira¹, Young-Hye Na³, Maxwell Giammona³, Antonio Mezzacapo⁴, Benjamin Wunsch⁵, Mathias Steiner^{1*}

¹IBM Research, Rio de Janeiro, 20031-170, RJ, Brazil.
 ²IBM Quantum, IBM Research - Almaden, San Jose, 95120, CA, USA.
 ³IBM Research, IBM Research - Almaden, San Jose, 95120, CA, USA.
 ⁴IBM Quantum, IBM T.J. Watson Research Center, Yorktown Heights, New York, 10598, NY, USA.

⁵IBM Research, IBM T.J. Watson Research Center, Yorktown Heights, New York, 10598, NY, USA.

*Corresponding author(s). E-mail(s): mathiast@br.ibm.com; Contributing authors: mabarroca@ibm.com;

Abstract

Accurate quantum chemistry calculations are essential for understanding electronic structures, yet exactly solving the many-body Schrödinger equation remains impractical due to electron correlation effects. While Density Functional Theory (DFT) is widely used, its inherent approximations limit its ability to capture strong correlation effects, particularly in surface reactions. Quantum computing offers a promising alternative, especially for localized electron interactions. In this work, we apply a quantum embedding approach to study the Oxygen Reduction Reaction at Lithium battery electrode surfaces. We employ an active space selection strategy, using Density Difference Analysis to identify key orbitals, which are subsequently refined with coupled-cluster natural orbitals. These are treated using Sample-Based Quantum Diagonalization (SQD) and its extended version (Ext-SQD), leveraging the Local Unitary Cluster Jastrow

⁶ Centro Brasileiro de Pesquisas Físicas, Rio de Janeiro, 22290-180, RJ, Brazil.

(LUCJ) ansatz for efficient state preparation on quantum hardware. Ext-SQD significantly improves upon standard SQD by incorporating excitation operators into the quantum-computed electron configurations used in classical Quantum Selected Configuration Interaction. Our approach demonstrates improved accuracy over Coupled Cluster Singles and Doubles (CCSD) calculations over ground state energies. The results, validated against Complete Active Space Configuration Interaction (CASCI), whenever computationally feasible, and Heat-Bath Configuration Interaction (HCI), provide new insights into $\text{Li}-\text{O}_2$ surface reactions, underscoring the potential of quantum computing in materials discovery and reaction modeling.

Keywords: Materials Science, Quantum Computing, Quantum Chemistry, Quantum Embedding

Introduction

Computational modeling of correlated electronic systems is essential for accurately predicting chemical and material properties. However, the exact solution of the electronic Schrödinger equation is computationally prohibitive, forcing the adoption of approximate methods. Although Density Functional Theory (DFT) is widely used, its exchange-correlation approximations struggle to capture strong electron-electron correlations in complex systems [1, 2].

Hybrid quantum-classical approaches, sometimes termed Quantum-centric Supercomputing [3], offer an alternative by leveraging quantum algorithms—such as Quantum Phase Estimation (QPE)—that, in principle, simulate electronic wavefunctions more efficiently than classical methods.[4–6] Due to current quantum hardware limitations, present approaches integrate quantum techniques with classical simulations. A critical aspect of these methods is active space selection, which reduces the computational burden while preserving key electronic correlations. Techniques like Density Difference Analysis (DDA), often refined with coupled-cluster natural orbitals [7], Atomic Valence Active Space (AVAS) [8], that creates an active space from a targeted set of atomic valence orbitals, and Density Matrix Embedding Theory (DMET)[9] which partitions the system into correlated fragments to attempt to capture electron correlation effects serve this purpose.

Traditional methods like the Variational Quantum Eigensolver (VQE)[10–12] have been explored for computing ground state energies, yet challenges related to ansatz design, barren plateaus, and high sampling overhead limit their scalability [13–16]. As a result, alternative approaches such as Sample-Based Quantum Diagonalization (SQD), a method that efficiently projects the electronic Hamiltonian onto a reduced subspace constructed from a sampled set of electronic configurations [17] and its enhanced version, Extended SQD (Ext-SQD), which introduces excitation operators to refine the configuration space and improve the accuracy of computed energy states.[18], have been developed to efficiently project the electronic Hamiltonian onto a reduced subspace. The configuration recovery process plays a crucial role in this

framework, iteratively correcting sampled electronic configurations to maintain the correct electron count and symmetry constraints, thereby ensuring reliable results.

To construct the reduced subspace for SQD and Ext-SQD, electronic configurations must be efficiently sampled from quantum hardware using an ansatz that balances physical accuracy with near-term feasibility. The Local Unitary Cluster Jastrow (LUCJ) ansatz achieves this by minimizing gate depth while preserving key correlation effects, and initializing circuits with classical coupled-cluster parameters further enhances configuration relevance [19]. Recent studies demonstrate that employing such ansätze on modern quantum processors enables accurate ground and excited state energy calculations under realistic conditions, paving the way for quantum-assisted electronic structure methods that surpass conventional classical approaches [17–20]. This integration with current quantum computing infrastructure highlights the applicability of these frameworks in real-world quantum simulations and paves the way for further improvements in quantum-assisted electronic structure calculations.

In this work, we leverage advanced hybrid quantum-classical methods designed for studying molecular reactions on surfaces relevant to battery materials, demonstrating that our hybrid quantum-classical framework achieves accurate ground-state energy calculations while remaining computationally efficient. We employ an active space selection method based on DDA [7] to identify the electronic orbitals most relevant for describing the reaction, we then build a LUCJ ansatz [19] within the active space and sample the most relevant configurations from this circuit on the ibm_torino processor. Afterwards we utilize SQD[17, 21] and Ext-SQD[18] to accurately compute reaction energy values.

Our results highlight the potential of integrating quantum computing with classical embedding techniques for advancing materials discovery and reaction modeling. By systematically selecting active spaces and leveraging sample-based diagonalization methods, we provide a scalable and effective approach for simulating complex chemical systems. In particular, we demonstrate that incorporating excitation operators in Ext-SQD significantly enhances the quality of sampled configuration spaces compared to standard SQD, leading to improved accuracy in representing ground state wavefunctions without entirely sacrificing computational efficiency. Finally, we discuss the broader implications of our work and propose directions for future research to further refine and scale quantum-assisted simulations in chemical and materials science.

Results

Reaction

The reaction between lithium and oxygen in Li-metal anode batteries plays a crucial role in stabilizing the solid electrolyte interface (SEI) and enhancing battery performance. While offering high energy density, Li-batteries face significant safety challenges due to dendrite formation, which can lead to short circuits and failure. The inclusion of dissolved oxygen in the electrolyte has been shown to mitigate dendrite growth by promoting the formation of lithium oxides, thereby improving stability and cycle life. [22]

The primary reaction of interest in these systems is

$$4 \operatorname{Li} + \operatorname{O}_2 \longrightarrow 2 \operatorname{Li}_2 \operatorname{O}$$
,

resulting in the formation of lithium oxide (Li_2O), which is deposited on the SEI. However, depending on local conditions such as oxygen concentration and electrolyte composition, other lithium oxides, including lithium peroxide (Li_2O_2) and lithium superoxide (Li_2O_2), may also form. The competition between these different reaction pathways is a critical factor influencing battery performance and longevity. [23, 24]

Previous studies have proposed reaction mechanisms for various surface-mediated electrochemical processes.[25, 26] Following a similar approach, we investigated the formation of ${\rm Li}^+$ and ${\rm O_2}^-$ species on the surface through quantum chemistry calculations. The reaction of lithium with oxygen involves the dissociation of molecular ${\rm O_2}$ and the subsequent adsorption of ${\rm O_2}^-$ anions, which interact with ${\rm Li}^+$ ions to form stable surface-bound lithium oxides. This process can be described by

$$Li + O_2 \longrightarrow Li^+ + O_2^-(ads).$$

The adsorption of ${\rm O_2}^-$ plays a critical role in the initial stages of lithium oxide formation. The stabilization of these anions on the surface dictates the pathway for further oxide growth, ultimately influencing the electrochemical performance of the battery. [23, 27, 28] By employing quantum simulations, we aim to capture the detailed electronic structure of these adsorbed species, providing insights into their stability and reactivity in lithium metal anode systems.

To study this system, we employed a computational workflow consisting of geometry optimization, active space selection, and quantum experiments. The workflow, summarized in Figure 1, enables a systematic investigation of lithium-oxygen interactions at the atomic level. The reaction energy was computed as the energy difference $\Delta E = E_{\rm prod} - E_{\rm reac}$ between the reactant and product states. This energy difference provides insights into the thermodynamics of lithium oxide formation, which is essential for understanding battery stability.

Geometry Optimization

The geometry optimizations were performed using DFT as implemented in the Vienna Ab initio Simulation Package (VASP) [29–31]. The structures were treated as periodic in the X-Y plane, with Li slab thickness of 6.1 Å and a vacuum layer of 12 Å along the Z direction to minimize interactions between periodic images. The Brillouin zone was sampled using a $4 \times 4 \times 1$ k-point grid within the Monkhorst-Pack scheme. Oxygen molecule was allowed to relax on the surface of Li slab to ensure an accurate representation of surface interactions. The inert core electrons were accounted by PAW pseudopotentials, and valence electrons were represented by plane-wave basis set. Only forces and geometries were allowed to relax while cell volume and shape was fixed. The convergence tolerance was set to 10^{-6} eV.

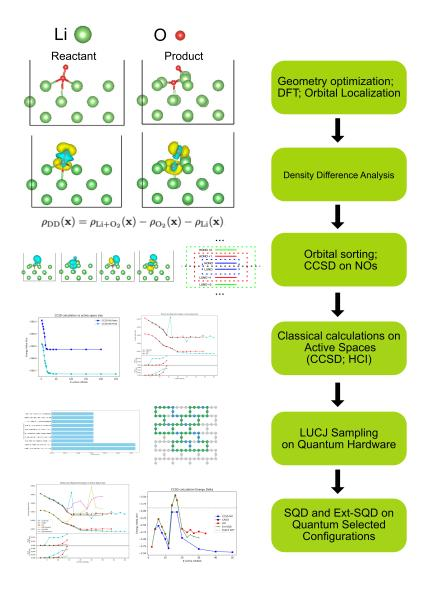


Fig. 1: Hybrid quantum-classical framework for studying lithium—oxygen reactions. Geometry optimization and DFT calculations lead into the Active space selection via DDA and Natural Orbitals which identifies the key orbitals, and a LUCJ ansatz samples configurations from quantum hardware. SQD/Ext-SQD then compute reaction energies ($\Delta E = E_{\rm prod} - E_{\rm reac}$), providing insights into lithium oxide formation.

Following geometry optimization, we utilized a Gaussian-type orbital (GTO) basis set, specifically the GTH-DZV basis set [32], in combination with the Perdew-Burke-Ernzerhof (PBE) exchange-correlation functional [33] and Goedecker-Teter-Hutter (GTH) pseudopotentials [32] to calculate the energy values and electronic density for both the reactant and product using DFT within the PySCF framework. [34] The electronic structure calculations were restricted to the Γ -point of the supercell, as including additional **k**-points did not significantly alter the electronic density.

The computed reaction energy at the Γ -point, namely $\Delta E = -3.897$ eV is underestimated against the typical literature values around -6 eV for Lithium oxides. [35–38]

Active Space Selection

The active space selection process combines multiple techniques to systematically identify the most relevant electronic orbitals for quantum simulations. First, Kohn-Sham orbitals are localized using the Pipek-Mezey method to preserve electronic structure characteristics across the Brillouin zone. This localization helps isolate occupied and virtual orbitals that contribute significantly to the reaction under study. Next, DDA is employed to assess charge redistribution by computing the electronic density difference between the reactant and product states. A tunable threshold function is then applied to filter out orbitals with negligible contributions, ensuring a physically meaningful selection of orbitals for the active space. Seven occupied orbitals are chosen for the reactant and eight for the product as well as all virtual orbitals. These choices were based on the valence space of O_2 and whether the computed electronic density for the orbitals was in the correct region.

To enhance accuracy and convergence, the selected active space is further refined using natural orbitals derived from coupled-cluster singles and doubles (CCSD) calculations in the active space previously formed. These orbitals are ranked based on occupation numbers, distinguishing those that are fully occupied, unoccupied, or fractionally occupied due to strong electron correlation effects. In our systems, we do not have fractionally occupied orbitals. The new active space is then constructed around the Highest Occupied Natural Orbital (HONO) and the Lowest Unoccupied Natural Orbital (LUNO), with additional orbitals included in an "inside-out" fashion as needed to improve accuracy and balance computational efficiency. This hierarchical selection approach ensures a compact yet sufficiently descriptive active space.

In Figure 2 we can see the Active Space selection procedure, the electronic density for the chosen systems, and some orbitals that comprise the product's active space.

Classical methods

Once the active-space orbitals were determined for the Γ -point, the rest were fixed and frozen at their Hartree-Fock (HF) levels, and the Born-Oppenheimer Hamiltonian was systematically reduced to the active space using established methods. We use the CCSD calculations of the active space Hamiltonian as a benchmark, as well

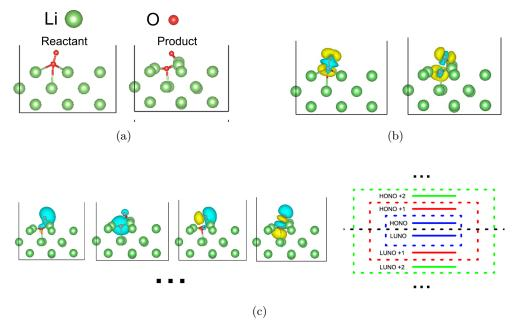


Fig. 2: Active Space selection We start with geometry optimization (a). Move to the Density difference analysis (b) and evaluate each orbital individual contribution to the density difference. Finally, we calculate the active space using the Natural Orbitals (c), where orbitals for the product are pictured. They were sorted based on their contribution to the Density difference. Natural Orbitals are calculated and the active space grows "inside out" from the HONO-LUNO level.

as Complete Active Space Configuration Interaction (CASCI) and Heat-bath Configuration Interaction (HCI) calculations, to serve as comparisons for the quantum methods. [39, 40]

In Figure 3 we can see the classical methods results. Energy values start to converge at around 20 orbitals and continue to slowly decrease up to 40 orbitals for both HCI and CCSD. This suggests that an active space of 40 orbitals would be necessary to calculate the energy difference. Due to computational resource limitations, we cannot scale CASCI beyond 14 orbitals but we can see reasonable agreement between the other two methods with errors within a few tens of mHa in this range. It is relevant as well that the error against CASCI increases as we add more orbitals to the active space, which is expected. As CCSD is not a variational method, it is possible that it actually underestimating the actual ground state energies that we have from HCI. In order to be sure, we need to look further at other more accurate variational methods, turns out that quantum experiments can provide us with that.

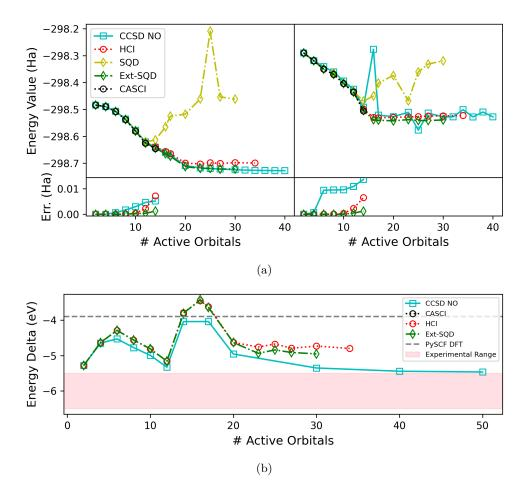


Fig. 3: Comparison of ground state and reaction energy results. (a) Quantum experiments and classical simulations of the ground state energies as a function of active space size. The left curves are for the product and the right ones are for the reactant. SQD and Ext-SQD results only scale up to 30 orbitals. (b) Reaction energies for quantum and classical methods computed at the Γ -point. DFT results are shown as a reference but are known to be overestimated.

Quantum methods

For the quantum experiments, the Hamiltonian was then reformulated in second quantization and converted into a qubit representation through standard fermion-to-qubit transformations. For this, we utilized the Jordan-Wigner (JW) encoding.

SQD projects the electronic Hamiltonian onto a subspace of sampled electronic configurations, ensuring proper electron count and spin sector. Similar to Quantum Selected Configuration Interaction (QSCI) [21], SQD systematically expands

the subspace for controlled accuracy improvements while maintaining computational feasibility. Our calculations involved 5-10 iterations with 16 batches per iteration.

To enhance sampling quality, we use a truncated Local Unitary Cluster Jastrow (LUCJ) ansatz [19], omitting final orbital rotations and Jastrow interactions to balance accuracy and efficiency. Circuits were built using the ffsim package and executed on the ibm_torino device, optimizing qubit selection based on calibration data in order to avoid qubits with higher error rates (Figure 4). Each circuit was sampled around 10⁶ times, and results were processed as bitstring distributions for SQD calculations.

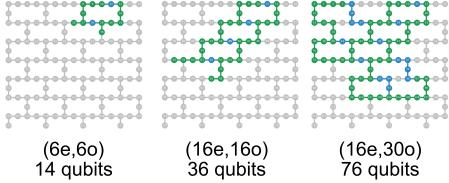


Fig. 4: **Circuit-to-chip mapping.** Green qubits represent spin orbitals while blue qubits act as ancillae. Numbers inside the qubits represent their index with respect to the device ordering.

In Figure 5 we can see histograms representing the output of the LUCJ circuit samples for the reactant in the (14e, 20o) active space. Notice that in Figure 5a the Hartree-Fock configuration is the most common, which happens when using a non-truncated one-layer LUCJ ansatz.[17] In Figure 5b we have the results for the truncated two-layer circuit, which leads to a more relevant distribution of configurations that is not dominated by the HF state. Therefore, we chose to use the truncated two-layer LUCJ ansatz for the rest of this work.

In Table 1 we see circuit sizes and qubit requirements for some of the circuits. Circuit size is described by depth and number of gates. When compared to previous work [17], we see our circuit requirements are similar for systems of comparable size. Bitstrings in the sampled distribution from ibm_torino that have forbidden configurations with incorrect Hamming weights, which appear due to noise, are on average 93.57% of the samples. This is around 10 times better than a uniform configuration distribution which sits at an average 99.922% of forbidden configurations. At the maximum value of 30 orbitals, circuits get considerably more complicated, with 2714 CX gates we are very close to the limits of what can give usable results on hardware before noise starts to prominently affect the bitstrings. The percentage now sits at 97.46% for the reactant and 98.32% for the product, which worsens calculated energy values for SQD ensuring results deteriorate for higher orbital counts, as can be seen in

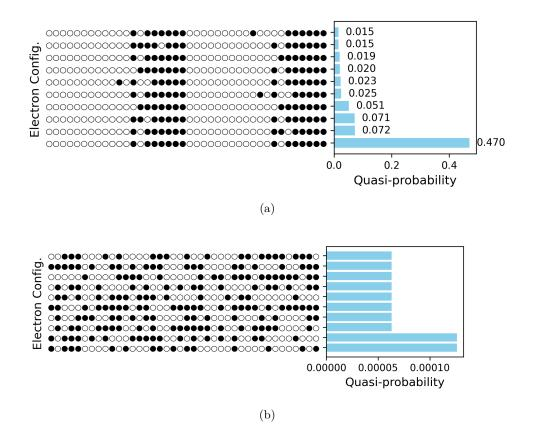


Fig. 5: Histograms of electron configurations sampled from the quantum hardware for the (14e,20o) reactant active space. We display only the top-10 configurations. Filled (unfilled) circles represent occupied (unoccupied) orbitals. (a) Histogram for the non-truncated one-layer LUCJ ansatz. (b) Histogram for the truncated two-layer LUCJ ansatz. We observe that the truncated variant leads to a more relevant distribution of electronic configurations, that is not dominated by the reference Hartree-Fock state.

Figure 3a. Fortunately, we can look beyond the standard SQD method with Ext-SQD, to enhance the accuracy of molecular ground-state energies.

Ext-SQD refines accuracy by applying excitation operators to sampled configurations [18]. Before applying these excitations, configurations in the wavefunction with amplitudes below a threshold of 10^{-2} are discarded, reducing computational cost while maintaining accuracy. The selection of which excitations to use can be adjusted as well to balance precision and efficiency, with higher-order excitations improving accuracy at an increased computational expense. To keep it manageable, we focus

Table 1: Quantum metrics for select circuits. q is the total number of qubits used, which is the sum of s qubits representing spin orbitals and a ancilla qubits. $|\tilde{\chi}|$ is the number of samples taken from <code>ibm_torino</code>, d is the 2-qubit circuit depth, CX is the number of CNOT gates and u the number of 1-qubit gates. Notice the small addition of two electrons in the product's active space makes circuits slightly larger after we include all occupied orbitals.

System	q(s+a)	$ ilde{oldsymbol{\chi}} $	d	CX	u
Prod(6e,6o)	14(12+2)	$1.5 \cdot 10^{6}$	38	132	262
Prod(12e, 12o)	30(24+6)	$1.5 \cdot 10^{6}$	64	474	943
Prod(16e,20o)	44(40+4)	$2 \cdot 10^{6}$	121	1252	2511
Prod(16e,30o)	76(60+16)	$2 \cdot 10^{6}$	298	2714	5455
Reac(6e,6o)	14(12+2)	$1.5\cdot 10^6$	38	132	262
Reac(12e,12o)	30(24+6)	$1.5 \cdot 10^{6}$	64	474	943
Reac(14e,20o)	44(40+4)	$2 \cdot 10^{6}$	112	1214	2443
Reac(14e,30o)	76(60+16)	$2 \cdot 10^6$	296	2648	5331

only on single excitations. Ext-SQD calculations do not rely on configuration recovery and simply start from the results from the previous SQD experiment, hence only one iteration is necessary. We keep the number of batches at 16.

Despite not providing accurate results, SQD is an integral step before starting the Ext-SQD calculation. Those, in turn, provide much better results, staying consistently closer to CASCI (below the 1.6 mHa chemical accuracy threshold) when compared to HCI and CCSD, at up to 14 orbitals, as seen in Figure 3a. Ext-SQD also reaches lower energy values for both the product and reactant beyond 14 orbitals. Unfortunately, scaling Ext-SQD beyond 30 orbitals proved challenging, but instead of the usual bottleneck in quantum resources, it now lies in the classical resources used during subspace diagonalization.

These calculations were conducted on standard x86 architecture CPU utilizing PySCF without any parallelization. Note on Table 2 that as the number of orbitals increases, the subspace dimension for Ext-SQD grows faster than for standard SQD. That is because the number of single excitations grows quadratically with the number of orbitals, which makes Ext-SQD challenging at higher orbital counts. [18]

On Figure 3b we plot the reaction energy up to 50 orbitals and provide the DFT value for reference. We can see HCI, Ext-SQD, and CCSD in this active space provide lower values which are more in line with those found in literature which, usually, rely on empirical corrections.[36–38, 41] We were unable to provide results up to 50 orbitals for all methods again due to a bottleneck on classical compute resources, but we can already see energy values starting to converge for both HCI and Ext-SQD earlier than CCSD. While CCSD seems to provide a ΔE value closer to what is expected from experiments it does so while overestimating reactant energy, so it cannot be taken at face value.

It is worth noting that while CCSD is not a variational method and can provide energy values below the actual ground state [42, 43], the same is not true for variational methods such as CASCI, HCI, and both SQD and Ext-SQD which are based upon CI methods. [17, 21] These methods can only find upper bounds for the actual ground

state energy for a given electronic Hamiltonian, which means lower energy values should always be more accurate.[43]

Table 2: Select Ext-SQD calculations for product and reactant. $|\tilde{\chi}|$ is the number of samples taken from **ibm torino**, K is the number of configuration recovery iterations used in SQD, D is the dimension of the subspace being diagonalized by SQD, while D_E is the dimension of the subspace being diagonalized by Ext-SQD.

System	$ ilde{\chi} $	K	D	D_E
Prod(2e,2o) Prod(12e,12o) Prod(16e,20o) Prod(16e,30o)	$\begin{aligned} 1.5 \cdot 10^6 \\ 1.5 \cdot 10^6 \\ 2 \cdot 10^6 \\ 2 \cdot 10^6 \end{aligned}$	5 7 10 10	$\begin{array}{c} 2.7 \cdot 10^4 \\ 3.4 \cdot 10^5 \\ 1.4 \cdot 10^6 \\ 1.4 \cdot 10^6 \end{array}$	$1.5 \cdot 10^4$ $2 \cdot 10^5$ $10 \cdot 10^6$ $23 \cdot 10^6$
Reac(2e,2o) Reac(12e,12o) Reac(14e,20o) Reac(14e,30o)	$1.5 \cdot 10^{6}$ $1.5 \cdot 10^{6}$ $2 \cdot 10^{6}$ $2 \cdot 10^{6}$	5 7 10 10	$2.9 \cdot 10^4$ $3.4 \cdot 10^5$ $1.3 \cdot 10^6$ $1.3 \cdot 10^6$	$ \begin{array}{r} 1.2 \cdot 10^4 \\ 1.8 \cdot 10^5 \\ 9 \cdot 10^6 \\ 28 \cdot 10^6 \end{array} $

Discussion

The results presented in this study demonstrate the potential of hybrid quantum-classical methods to improve the accuracy of electronic structure calculations for surface reactions relevant to battery materials. By leveraging a systematic active space selection approach and employing SQD alongside Ext-SQD, we were able to compute ground-state energies with better accuracy compared to conventional classical methods such as HCI and CCSD. The agreement between Ext-SQD and CASCI at small active spaces, coupled with its ability to scale close to 30 orbitals, highlights its utility for studying strongly correlated electronic systems.

Our methodology, as described in Figure 1 effectively integrates classical and quantum techniques to achieve computationally efficient simulations. The use of DDA and natural orbitals from coupled-cluster calculations ensures that the active space captures the most relevant electronic degrees of freedom. The refinement of active spaces using coupled-cluster natural orbitals improves convergence and enhances the accuracy of quantum calculations. This approach is particularly advantageous for studying reactions at interfaces, where electronic correlation effects play a crucial role.

The integration of quantum computing hardware allowed us to validate our methods in a real quantum processor. As shown in Table 1, circuit depths and gate counts increase significantly as the number of orbitals grows, emphasizing the challenge of scaling quantum simulations on current hardware. The results obtained from executing LUCJ circuits confirm that our approach is feasible on near-term quantum devices, but further noise mitigation strategies will be necessary to maintain accuracy at larger system sizes.

One key finding of our study is that Ext-SQD provides a significant improvement over standard SQD by incorporating excitation operators to refine the sampled configuration space. This enhancement allows for better representation of ground-state

wavefunctions while maintaining computational feasibility. However, as indicated in Figure 3a, the computational cost associated with Ext-SQD grows significantly as the number of orbitals increases, shifting the bottleneck from quantum resources to classical diagonalization routines. Future work should focus on optimizing classical post-processing techniques, such as parallelizing the diagonalization of extended subspaces, to enable simulations with larger active spaces. These optimizations could allows us to scale beyond 30 orbitals up to around 40 orbitals where the bottleneck shifts back to the quantum stack.

Another important aspect of our results is the comparison with classical methods. Figure 3 illustrates how Ext-SQD converges to lower energy values compared to CCSD and HCI, at around 20 orbitals. This suggests that quantum methods, when properly integrated with classical solvers, can offer tangible improvements in computational chemistry for materials discovery. Additionally, the energy differences computed with Ext-SQD begin to converge earlier than those from CCSD, reinforcing the advantages of this quantum-classical approach.

Despite these advancements, several challenges must be addressed before quantum-assisted simulations become a practical tool for real-world applications. Noise resilience, circuit depth limitations, and efficient state preparation remain key hurdles. The LUCJ ansatz, while effective in reducing circuit depth, may require further modifications to enhance expressivity and error resilience. Additionally, exploring alternative quantum ansatzes, such as adaptive variational circuits, could further improve energy estimations while maintaining hardware efficiency.

Looking ahead, the insights gained from this work provide a strong foundation for future research in quantum-assisted simulations of surface reactions. The extension of our approach to more complex reaction networks, multi-step catalytic processes, and beyond lithium-oxygen systems will be an important direction. As quantum hardware continues to advance, the scalability of hybrid methods like Ext-SQD will be further tested, paving the way for practical quantum chemistry applications in energy storage and materials science.

In conclusion, this study demonstrates that hybrid quantum-classical methodologies, particularly those leveraging advanced active space selection and sample-based diagonalization techniques, offer a promising path forward for studying complex chemical systems. While challenges remain, our results underscore the potential of quantum computing to complement and extend classical approaches, bringing us closer to achieving accurate and efficient electronic structure calculations for materials discovery.

Methods

DFT Energy Calculations

Repeating the procedure established in previous work [7], after geometry optimization, we conducted DFT calculations utilizing a basis formed by translationally adapted linear combinations of Gaussian atomic orbitals (AOs). This basis is expressed as:

$$\phi_{k,p}(r) = \sum_{T} e^{ik \cdot T} \chi_p(r - T), \tag{1}$$

where $T = \sum_{i=1}^{3} T_i a_i$ represents a lattice translation vector, $k = \sum_{i=1}^{3} k_i b_i$ denotes a momentum vector within the first Brillouin zone, and χ_p is a Gaussian-type atomic orbital. The summation over T ensures that the constructed orbitals respect the translational periodicity of the system.[44, 45]

All electronic structure calculations were performed using the PySCF package [34], again employing the GTH-DZV basis set [32] alongside the Goedecker-Teter-Hutter (GTH) pseudopotentials [32] and the Perdew-Burke-Ernzerhof (PBE) exchange-correlation functional [33].

Within this basis, the Born-Oppenheimer Hamiltonian takes the following representation:[46]

$$\hat{H} = E_0 + \sum_{\substack{\mathbf{k} \\ pr\sigma}} h_{pr}(\mathbf{k}) \hat{a}_{\mathbf{k}p\sigma}^{\dagger} \hat{a}_{\mathbf{k}r\sigma} + \sum_{\substack{\mathbf{k}_{\mathbf{p}}, \mathbf{k}_{\mathbf{r}}, \mathbf{k}_{\mathbf{q}}, \mathbf{k}_{\mathbf{s}} \\ prqs\sigma\tau}}^{*} \frac{(\mathbf{k}_{\mathbf{p}}p, \mathbf{k}_{\mathbf{r}}r | \mathbf{k}_{\mathbf{q}}q, \mathbf{k}_{\mathbf{s}}s)}{2} \hat{a}_{\mathbf{k}_{\mathbf{p}}p\sigma}^{\dagger} \hat{a}_{\mathbf{k}_{\mathbf{q}}q\tau} \hat{a}_{\mathbf{k}_{\mathbf{s}}s\tau} \hat{a}_{\mathbf{k}_{\mathbf{r}}r\sigma},$$

where momentum conservation is enforced such that $k_p + k_q - k_r - k_s = G$, with G being a reciprocal lattice vector. To efficiently approximate electron-electron interactions, we employed density fitting with a Weigend auxiliary basis.

Active Space Selection

We localized the Kohn-Sham orbitals using the Pipek-Mezey method [47], which relies on a Mulliken population analysis with meta-Löwdin orbitals [48, 49]. Localization was performed separately for occupied and virtual orbitals at each individual **k**-point to ensure that the electronic structure characteristics were properly preserved across the Brillouin zone. We computed the electronic density difference at the DFT level, as defined by

$$\rho_{\rm DD}(\mathbf{x}) = |\rho_{\rm Li+O_2}(\mathbf{x}) - \rho_{\rm O_2}(\mathbf{x}) - \rho_{\rm Li}(\mathbf{x})|,\tag{3}$$

which provides insights into charge redistribution during the reaction and is included in Figure 2b.

To automate the selection of the active space, we ranked orbitals based on their contributions to the density difference. To quantify these contributions, we introduced a threshold parameter η that suppresses minor orbital components and retains only physically meaningful orbitals. By systematically varying this threshold, we identified a stable range where orbital rankings remain consistent, facilitating a robust and physically motivated selection of the active space. To mitigate this sensitivity, we identified a stable range of $\eta \approx 10^{-3}$ through a systematic scan. Within this range, the ranking of occupied localized orbitals remains stable, allowing for a selection of the most relevant orbitals for further quantum simulations.

To further enhance active space selection and ensure convergence with respect to active space size, we combined this density difference analysis with natural orbitals

obtained from CCSD calculations. Specifically, an initial CCSD calculation was performed within an active space constructed from the highest-ranked occupied orbitals identified via the density difference analysis and all virtual orbitals. The resulting natural orbitals exhibit occupation numbers predominantly close to either zero or two, clearly distinguishing high-occupancy orbitals from low-occupancy ones. In cases involving stronger electron correlation, orbitals with fractional occupancy must be explicitly included. The final active space was systematically constructed around the Highest Occupied Natural Orbital (HONO) and the Lowest Unoccupied Natural Orbital (LUNO).

For more details on the active space selection method, please refer to the original publication [7].

Quantum Simulations

The Sample-Based Quantum Diagonalization (SQD) [17, 21, 50] approach involves projecting the electronic Hamiltonian onto a subspace defined by a collection of electronic configurations sampled from a probability distribution. These set of configurations, denoted as $X = \{x\}$, are drawn from the wavefunction probability $P_{\Psi}(x) = |\langle x|\Psi\rangle|^2$, whereas a noisy version is represented by $P_{\tilde{\Psi}}(x) = \langle x|\tilde{\rho}|x\rangle$. The subset of configurations that maintain the correct particle number is labeled X_N , and through a self-consistent recovery process, an expanded configuration set X_R is constructed. The electronic Hamiltonian \hat{H} is then projected onto this selected subspace, and its low-energy eigenvalues and eigenvectors are determined via direct diagonalization using the iterative Davidson algorithm[51] across multiple classical computing nodes [17].

To obtain the set of configurations, we sample a relevant circuit, an ansatz, on a quantum device. The Local Unitary Cluster Jastrow (LUCJ) [19] ansatz is a variational quantum circuit designed to generate approximate ground states of electronic systems while maintaining a moderate circuit depth. It is derived from unitary coupled-cluster (UCC) theory but incorporates local approximations to reduce the number of required two-qubit gates, making it more suitable for near-term quantum devices. The LUCJ wavefunction is constructed as

$$|\Psi\rangle = \prod_{\mu=1}^{L} e^{\hat{K}_{\mu}} e^{i\hat{J}_{\mu}} e^{-\hat{K}_{\mu}} |x_{\text{RHF}}\rangle, \tag{4}$$

where $\hat{K}_{\mu} = \sum_{pr,\sigma} K^{\mu}_{pr} \hat{a}^{\dagger}_{p\sigma} \hat{a}_{r\sigma}$ are one-body excitation operators, $\hat{J}_{\mu} = \sum_{pr,\sigma\tau} J^{\mu}_{p\sigma,r\tau} \hat{n}_{p\sigma} \hat{n}_{r\tau}$ are density-density interactions and $|x_{\rm RHF}\rangle$ represents the reference Hartree-Fock (RHF) state encoded in the Jordan-Wigner mapping.

The circuit depth can be further reduced, while preserving key dynamical correlations, by employing a truncated version of the LUCJ ansatz. Specifically, we used the form

$$|\Psi\rangle = e^{\hat{K}_2} e^{-\hat{K}_1} e^{i\hat{J}_1} e^{\hat{K}_1} |x_{\text{RHF}}\rangle. \tag{5}$$

which corresponds to a two-layer LUCJ circuit where the final orbital rotation $e^{\hat{K}_2}$ and Jastrow interaction $e^{i\hat{J}_2}$ are omitted, reducing the circuit depth to that of a

single-layer LUCJ. The truncation significantly decreases computational costs while retaining enough flexibility to capture electron correlation effects.[17]

We employed an extension of the SQD method, termed Extended SQD (Ext-SQD), to obtain more accurate molecular ground-state energies. While most of the time, the standard SQD method effectively estimates ground-state properties by constructing a subspace from sampled computational basis states, its reliance on configurations drawn from a quantum circuit approximating the ground state introduces a bias that can lead to an overestimation of the energies. [18] To address these limitations, Ext-SQD incorporates elements of Quantum Subspace Expansion (QSE) while maintaining the computational efficiency of SQD. In contrast to standard SQD, which forms excited states by solving for multiple eigenpairs of a projected Hamiltonian, Ext-SQD expands the accessible configuration space by explicitly applying excitation operators to the computational basis states in the original subspace.

Acknowledgments. We want to acknowledge Ben Jaderberg, Edward Chen, Mario Motta, Mirko Armico, Gavin Jones, Ieva Liepuoniute, Kevin Sung, Javier Robledo Moreno, Kunal Sharma, and Petar Jurcevic for the meaningful discussions and assistance.

Declarations

Code availability. Here is a list of all open source code repositories used in this work: PYSCF [34], Ffsim [52], Qiskit SDK [53], Qiskit addons sqd [54], Ray [55] Closed-source software includes the VASP (Vienna Ab initio Simulation Package).[29][30][31]

References

- [1] Cohen, A.J., Mori-Sánchez, P., Yang, W.: Insights into current limitations of density functional theory. Science https://doi.org/10.1126/science.1158722 792 - 794(2008)**321**(5890), https://www.science.org/doi/pdf/10.1126/science.1158722
- Jones, R.O., Gunnarsson, O.: The density functional formalism, its applications and prospects. Rev. Mod. Phys. 61, 689-746 (1989) https://doi.org/10.1103/ RevModPhys.61.689
- [3] Alexeev, Y., Amsler, M., Barroca, M.A., Bassini, S., Battelle, T., Camps, D., Casanova, D., Choi, Y.J., Chong, F.T., Chung, C., Codella, C., Córcoles, A.D., Cruise, J., Di Meglio, A., Duran, I., Eckl, T., Economou, S., Eidenbenz, S., Elmegreen, B., Fare, C., Faro, I., Fernández, C.S., Ferreira, R.N.B., Fuji, K., Fuller, B., Gagliardi, L., Galli, G., Glick, J.R., Gobbi, I., Gokhale, P., Puente Gonzalez, S., Greiner, J., Gropp, B., Grossi, M., Gull, E., Healy, B., Hermes, M.R., Huang, B., Humble, T.S., Ito, N., Izmaylov, A.F., Javadi-Abhari, A., Jennewein, D., Jha, S., Jiang, L., Jones, B., Jong, W.A., Jurcevic, P., Kirby, W., Kister, S., Kitagawa, M., Klassen, J., Klymko, K., Koh, K., Kondo, M., Kürkçüoğlu,

- D.g.M., Kurowski, K., Laino, T., Landfield, R., Leininger, M., Leyton-Ortega, V., Li, A., Lin, M., Liu, J., Lorente, N., Luckow, A., Martiel, S., Martin-Fernandez, F., Martonosi, M., Marvinney, C., Medina, A.C., Merten, D., Mezzacapo, A., Michielsen, K., Mitra, A., Mittal, T., Moon, K., Moore, J., Mostame, S., Motta, M., Na, Y.-H., Nam, Y., Narang, P., Ohnishi, Y.-Y., Ottaviani, D., Otten, M., Pakin, S., Pascuzzi, V.R., Pednault, E., Piontek, T., Pitera, J., Rall, P., Ravi, G.S., Robertson, N., Rossi, M.A.C., Rydlichowski, P., Ryu, H., Samsonidze, G., Sato, M., Saurabh, N., Sharma, V., Sharma, K., Shin, S., Slessman, G., Steiner, M., Sitdikov, I., Suh, I.-S., Switzer, E.D., Tang, W., Thompson, J., Todo, S., Tran, M.C., Trenev, D., Trott, C., Tseng, H.-H., Tubman, N.M., Tureci, E., Valiñas, D.G., Vallecorsa, S., Wever, C., Wojciechowski, K., Wu, X., Yoo, S., Yoshioka, N., Yu, V.W.-Z., Yunoki, S., Zhuk, S., Zubarev, D.: Quantum-centric supercomputing for materials science: A perspective on challenges and future directions. Future Gener. Comput. Syst. 160, 666–710 (2024)
- [4] Kang, C., Bauman, N.P., Krishnamoorthy, S., Kowalski, K.: Optimized quantum phase estimation for simulating electronic states in various energy regimes. Journal of Chemical Theory and Computation 18(11), 6567–6576 (2022) https://doi. org/10.1021/acs.jctc.2c00577 https://doi.org/10.1021/acs.jctc.2c00577. PMID: 36201845
- [5] Cortes, C.L., Rocca, D., Gonthier, J., Ollitrault, P.J., Parrish, R.M., Anselmetti, G.-L.R., Degroote, M., Moll, N., Santagati, R., Streif, M.: Assessing the query complexity limits of quantum phase estimation using symmetry aware spectral bounds (2024). https://arxiv.org/abs/2403.04737
- [6] Goings, J.J., White, A., Lee, J., Tautermann, C.S., Degroote, M., Gidney, C., Shiozaki, T., Babbush, R., Rubin, N.C.: Reliably assessing the electronic structure of cytochrome p450 on today's classical computers and tomorrow's quantum computers. Proceedings of the National Academy of Sciences 119(38), 2203533119 (2022) https://doi.org/10.1073/pnas.2203533119 https://www.pnas.org/doi/pdf/10.1073/pnas.2203533119
- [7] Gujarati, T.P., Motta, M., Friedhoff, T.N., Rice, J.E., Nguyen, N., Barkoutsos, P.K., Thompson, R.J., Smith, T., Kagele, M., Brei, M., Jones, B.A., Williams, K.: Quantum computation of reactions on surfaces using local embedding. npj Quantum Information 9(1) (2023) https://doi.org/10.1038/s41534-023-00753-1
- [8] Sayfutyarova, E.R., Sun, Q., Chan, G.K.-L., Knizia, G.: Automated construction of molecular active spaces from atomic valence orbitals. J. Chem. Theory Comput. 13(9), 4063–4078 (2017)
- [9] Sun, Q., Chan, G.K.-L.: Exact and optimal quantum mechanics/molecular mechanics boundaries. J. Chem. Theory Comput. 10(9), 3784–3790 (2014)
- [10] Peruzzo, A., McClean, J., Shadbolt, P., Yung, M.-H., Zhou, X.-Q., Love, P.J., Aspuru-Guzik, A., O'Brien, J.L.: A variational eigenvalue solver on a photonic

- quantum processor. Nature Communications **5**(1), 4213 (2014) https://doi.org/10.1038/ncomms5213
- [11] Reiher, M., Wiebe, N., Svore, K.M., Wecker, D., Troyer, M.: Elucidating reaction mechanisms on quantum computers. Proceedings of the National Academy of Sciences 114(29), 7555–7560 (2017) https://doi.org/10.1073/pnas.1619152114 https://www.pnas.org/doi/pdf/10.1073/pnas.1619152114
- [12] Wecker, D., Bauer, B., Clark, B.K., Hastings, M.B., Troyer, M.: Gate-count estimates for performing quantum chemistry on small quantum computers. Phys. Rev. A 90, 022305 (2014) https://doi.org/10.1103/PhysRevA.90.022305
- [13] Fedorov, D.A., Peng, B., Govind, N., Alexeev, Y.: VQE method: a short survey and recent developments. Mater. Theory 6(1) (2022)
- [14] Clary, J.M., Jones, E.B., Vigil-Fowler, D., Chang, C., Graf, P.: Exploring the scaling limitations of the variational quantum eigensolver with the bond dissociation of hydride diatomic molecules. Int. J. Quantum Chem. **123**(11) (2023)
- [15] Holmes, Z., Sharma, K., Cerezo, M., Coles, P.J.: Connecting ansatz expressibility to gradient magnitudes and barren plateaus. PRX Quantum 3, 010313 (2022) https://doi.org/10.1103/PRXQuantum.3.010313
- [16] Singkanipa, P., Lidar, D.A.: Beyond unital noise in variational quantum algorithms: noise-induced barren plateaus and limit sets. Quantum **9**(1617), 1617 (2025)
- [17] Robledo-Moreno, J., Motta, M., Haas, H., Javadi-Abhari, A., Jurcevic, P., Kirby, W., Martiel, S., Sharma, K., Sharma, S., Shirakawa, T., Sitdikov, I., Sun, R.-Y., Sung, K.J., Takita, M., Tran, M.C., Yunoki, S., Mezzacapo, A.: Chemistry Beyond Exact Solutions on a Quantum-Centric Supercomputer (2024). https://arxiv.org/abs/2405.05068
- [18] Barison, S., Moreno, J.R., Motta, M.: Quantum-centric computation of molecular excited states with extended sample-based quantum diagonalization (2024). https://arxiv.org/abs/2411.00468
- [19] Motta, M., Sung, K.J., Whaley, K.B., Head-Gordon, M., Shee, J.: Bridging physical intuition and hardware efficiency for correlated electronic states: the local unitary cluster jastrow ansatz for electronic structure. Chem. Sci. 14, 11213–11227 (2023) https://doi.org/10.1039/D3SC02516K
- [20] Liepuoniute, I., Doney, K.D., Robledo-Moreno, J., Job, J.A., Friend, W.S., Jones, G.O.: Quantum-Centric Study of Methylene Singlet and Triplet States (2024). https://arxiv.org/abs/2411.04827
- [21] Kanno, K., Kohda, M., Imai, R., Koh, S., Mitarai, K., Mizukami, W., Nakagawa,

- Y.O.: Quantum-Selected Configuration Interaction: classical diagonalization of Hamiltonians in subspaces selected by quantum computers (2023). https://arxiv.org/abs/2302.11320
- [22] Giammona, M.J., Kim, J., Kim, Y., Medina, P., Nguyen, K., Bui, H., Jones, G.O., Tek, A.T., Sundberg, L., Fong, A., La, Y.-H.: Oxygen assisted lithium-iodine batteries: Towards practical iodine cathodes and viable lithium metal protection strategies. Adv. Mater. Interfaces 10(17) (2023)
- [23] Giordani, V., Walker, W., Bryantsev, V.S., Uddin, J., Chase, G.V., Addison, D.: Synergistic effect of oxygen and LiNO3on the interfacial stability of lithium metal in a Li/O2Battery. J. Electrochem. Soc. 160(9), 1544–1550 (2013)
- [24] Zheng, S., Geng, H., Eliseeva, S.N., Wang, B.: Air-exposed lithium metal as a highly stable anode for low-temperature energy storage applications. Energy Materials 2(6) (2022) https://doi.org/10.20517/energymater.2022.66
- [25] Ince, J., Peerzada, M., Mathews, L., Pai, A., Al-Qatatsheh, A., Abbasi, S., Yin, Y., Hameed, N., Duffy, A., Lau, A., Salim, N.: Overview of emerging hybrid and composite materials for space applications. Advanced Composites and Hybrid Materials 6, 130 (2023) https://doi.org/10.1007/s42114-023-00678-5
- [26] Liu, T., Zhao, S., Xiong, Q., Yu, J., Wang, J., Huang, G., Ni, M., Zhang, X.: Reversible Discharge Products in Li-Air Batteries. Advanced Materials 35 (2023) https://doi.org/10.1002/adma.202208925
- [27] Shen, C., Yan, H., Gu, J., Gao, Y., Yang, J., Xie, K.: Li2O-reinforced solid electrolyte interphase on three-dimensional sponges for dendrite-free lithium deposition. Front. Chem. 6, 517 (2018)
- [28] Wang, E., Dey, S., Liu, T., Menkin, S., Grey, C.P.: Effects of atmospheric gases on li metal cyclability and solid-electrolyte interphase formation. ACS Energy Lett. 5(4), 1088–1094 (2020)
- [29] Kresse, G., Hafner, J.: Ab initio molecular dynamics for liquid metals. Phys. Rev. B 47, 558–561 (1993)
- [30] Kresse, G., Furthmüller, J.: Efficiency of ab-initio total energy calculations for metals and semiconductors using a plane-wave basis set. Comput. Mater. Sci. 6, 15–50 (1996)
- [31] Kresse, G., Joubert, D.: From ultrasoft pseudopotentials to the projector augmented-wave method. Phys. Rev. B **59**, 1758–1775 (1999)
- [32] Goedecker, S., Teter, M., Hutter, J.: Separable dual-space gaussian pseudopotentials. Phys. Rev. B **54**, 1703–1710 (1996) https://doi.org/10.1103/PhysRevB.54. 1703

- [33] Perdew, J.P., Burke, K., Ernzerhof, M.: Generalized gradient approximation made simple. Phys. Rev. Lett. 77, 3865–3868 (1996) https://doi.org/10.1103/ PhysRevLett.77.3865
- [34] Sun, Q., Berkelbach, T.C., Blunt, N.S., Booth, G.H., Guo, S., Li, Z., Liu, J., McClain, J.D., Sayfutyarova, E.R., Sharma, S., Wouters, S., Chan, G.K.-L.: Pyscf: the python-based simulations of chemistry framework. WIREs Computational Molecular Science 8(1), 1340 (2018) https://doi.org/10.1002/wcms.1340 https://wires.onlinelibrary.wiley.com/doi/pdf/10.1002/wcms.1340
- [35] Chase, M.: NIST-JANAF Thermochemical Tables, 4th Edition. American Institute of Physics, -1, ??? (1998)
- [36] Radin, M.D., Rodriguez, J.F., Tian, F., Siegel, D.J.: Lithium peroxide surfaces are metallic, while lithium oxide surfaces are not. Journal of the American Chemical Society 134(2), 1093–1103 (2012) https://doi.org/10.1021/ja208944x https://doi.org/10.1021/ja208944x. PMID: 22148314
- [37] Hummelshøj, J.S., Blomqvist, J., Datta, S., Vegge, T., Rossmeisl, J., Thygesen, K.S., Luntz, A.C., Jacobsen, K.W., Nørskov, J.K.: Communications: Elementary oxygen electrode reactions in the aprotic li-air battery. J. Chem. Phys. 132(7), 071101 (2010)
- [38] Seriani, N.: Ab initio thermodynamics of lithium oxides: from bulk phases to nanoparticles. Nanotechnology **20**(44), 445703 (2009)
- [39] Boguslawski, K., Marti, K.H., Reiher, M.: Construction of casci-type wave functions for very large active spaces. The Journal of Chemical Physics 134(22) (2011) https://doi.org/10.1063/1.3596482
- [40] Holmes, A.A., Tubman, N.M., Umrigar, C.J.: Heat-bath configuration interaction: An efficient selected configuration interaction algorithm inspired by heat-bath sampling. J. Chem. Theory Comput. 12(8), 3674–3680 (2016)
- [41] Galloway, T.A., Dong, J.-C., Li, J.-F., Attard, G., Hardwick, L.J.: Oxygen reactions on pt{hkl} in a non-aqueous na+ electrolyte: site selective stabilisation of a sodium peroxy species. Chem. Sci. **10**(10), 2956–2964 (2019)
- [42] Cremer, D.: From configuration interaction to coupled cluster theory: The quadratic configuration interaction approach. Wiley Interdiscip. Rev. Comput. Mol. Sci. **3**(5), 482–503 (2013)
- [43] Helgaker, T., Jørgensen, P., Olsen, J.: Molecular Electronic Structure Theory. John Wiley & Sons, LTD, Chichester (2000)

- [44] McClain, J., Sun, Q., Chan, G.K.-L., Berkelbach, T.C.: Gaussian-based coupled-cluster theory for the ground-state and band structure of solids. Journal of Chemical Theory and Computation 13(3), 1209–1218 (2017) https://doi.org/10.1021/acs.jctc.7b00049 https://doi.org/10.1021/acs.jctc.7b00049. PMID: 28218843
- [45] Dovesi, R., Civalleri, B., Roetti, C., Saunders, V.R., Orlando, R.: 1. Ab Initio Quantum Simulation in Solid State Chemistry, pp. 1–125. John Wiley & Sons, Ltd, ??? (2005). https://doi.org/10.1002/0471720895.ch1 . https://onlinelibrary.wiley.com/doi/abs/10.1002/0471720895.ch1
- [46] VandeVondele, J., Krack, M., Mohamed, F., Parrinello, M., Chassaing, T., Hutter, J.: Quickstep: Fast and accurate density functional calculations using a mixed gaussian and plane waves approach. Computer Physics Communications 167(2), 103–128 (2005) https://doi.org/10.1016/j.cpc.2004.12.014
- [47] Pipek, J., Mezey, P.G.: A fast intrinsic localization procedure applicable for ab-initio and semiempirical linear combination of atomic orbital wave functions. The Journal of Chemical Physics 90(9), 4916–4926 (1989) https://doi.org/10.1063/1.456588 https://pubs.aip.org/aip/jcp/article-pdf/90/9/4916/18976237/4916_1_online.pdf
- [48] Sun, Q., Chan, G.K.-L.: Exact and optimal quantum mechanics/molecular mechanics boundaries. Journal of Chemical Theory and Computation 10(9), 3784–3790 (2014) https://doi.org/10.1021/ct500512f https://doi.org/10.1021/ct500512f. PMID: 26588523
- [49] Lehtola, S., Jónsson, H.: Pipek-mezey orbital localization using various partial charge estimates. Journal of Chemical Theory and Computation 10(2), 642–649 (2014) https://doi.org/10.1021/ct401016x https://doi.org/10.1021/ct401016x. PMID: 26580041
- [50] Nützel, L., Gresch, A., Hehn, L., Marti, L., Freund, R., Steiner, A., Marciniak, C.D., Eckstein, T., Stockinger, N., Wolf, S., Monz, T., Kühn, M., Hartmann, M.J.: Solving an industrially relevant quantum chemistry problem on quantum hardware. Quantum Science and Technology 10(1), 015066 (2025) https://doi.org/10.1088/2058-9565/ad9ed3
- [51] Crouzeix, M., Philippe, B., Sadkane, M.: The davidson method. SIAM Journal on Scientific Computing 15(1), 62–76 (1994) https://doi.org/10.1137/0915004 https://doi.org/10.1137/0915004
- [52] The ffsim developers: ffsim: Faster Simulations of Fermionic Quantum Circuits. https://github.com/qiskit-community/ffsim
- [53] Javadi-Abhari, A., Treinish, M., Krsulich, K., Wood, C.J., Lishman, J., Gacon, J., Martiel, S., Nation, P.D., Bishop, L.S., Cross, A.W., Johnson, B.R., Gambetta, J.M.: Quantum computing with Qiskit (2024). https://arxiv.org/abs/2405.08810

- [54] Saki, A.A., Barison, S., Fuller, B., Garrison, J.R., Glick, J.R., Johnson, C., Mezzacapo, A., Robledo-Moreno, J., Rossmannek, M., Schweigert, P., Sitdikov, I., Sung, K.J.: Qiskit Addon: Sample-based Quantum Diagonalization
- [55] Moritz, P., Nishihara, R., Wang, S., Tumanov, A., Liaw, R., Liang, E., Elibol, M., Yang, Z., Paul, W., Jordan, M.I., Stoica, I.: Ray: A Distributed Framework for Emerging AI Applications (2018). https://arxiv.org/abs/1712.05889